

# The XM M -LSS survey

## I. Scientific motivations, design and first results<sup>?</sup>

M. Pierre<sup>1</sup>, I. Valtchanov<sup>1</sup>, S. Dos Santos<sup>1</sup>, B. Altieri<sup>2</sup>, S. Andreon<sup>3</sup>, M. Bolzonella<sup>4</sup>, M. Bremer<sup>5</sup>, C. Jean<sup>6</sup>, A. M. Read<sup>7</sup>, A. Refregier<sup>1</sup>, J. W. Ellis<sup>8,14</sup>, C. Adam<sup>9</sup>, D. A. Llois<sup>8</sup>, M. Birkshaw<sup>5</sup>, L. Chiappetti<sup>4</sup>, A. Cohen<sup>10</sup>, A. D'Elia<sup>6</sup>, P. A. Duc<sup>1</sup>, E. G. Osset<sup>6</sup>, L. R. Jones<sup>7</sup>, O. Le Fevre<sup>9</sup>, D. Maccagni<sup>4</sup>, B. Maccagni<sup>12</sup>, H. Maccracken<sup>9</sup>, Y. Mellier<sup>13</sup>, T. J. Ponman<sup>7</sup>, H. Quintana<sup>14</sup>, H. Rottgering<sup>15</sup>, A. Smette<sup>6</sup>, J. Surdej<sup>6</sup>, L. Vigroux<sup>1</sup>, H. Boehringer<sup>17</sup>, J. H. Barth<sup>18</sup>, C. Lonsdale<sup>11</sup>, and S. D. M. White<sup>16</sup>

<sup>1</sup> CEA/DAM/DAPNIA, Service d'Astrophysique, Saclay, F-91191 Gif sur Yvette

<sup>2</sup> XM M Science Operations Centre, Villafranca, Spain

<sup>3</sup> Osservatorio Astronomico di Brera, Milano, Italy

<sup>4</sup> INFN, Milano, Italy

<sup>5</sup> Department of Physics, University of Bristol, UK

<sup>6</sup> Institut d'Astrophysique et de Geophysique, Universite de Liege, Belgium

<sup>7</sup> School of Physics and Astronomy, University of Birmingham, UK

<sup>8</sup> European Southern Observatory, Santiago, Chile

<sup>9</sup> Laboratoire d'Astrophysique, Marseille, France

<sup>10</sup> Naval Research Laboratory, Washington, US

<sup>11</sup> Infrared Processing and Analysis Center, Caltech, US

<sup>12</sup> Physics Department, University College, Dublin, Ireland

<sup>13</sup> Institut d'Astrophysique, Paris, France

<sup>14</sup> Pontificia Universidad Catolica, Santiago, Chile

<sup>15</sup> Leiden Observatory, Leiden, The Netherlands

<sup>16</sup> Max Planck Institut für Extraterrestrische Physik, Garching bei München, Germany.

<sup>17</sup> Max Planck Institut für Astrophysik, Garching bei München, Germany.

<sup>18</sup> Astronomical Observatory, Copenhagen, Denmark

Received April 2003

**Abstract.** We have designed a medium deep large area X-ray survey with XM M (the XM M Large Scale Structure survey, XM M -LSS) with the scope of extending the cosmological tests attempted using ROSAT cluster samples to two redshift bins between  $0 < z < 1$  while maintaining the precision of earlier studies. Two main goals have constrained the survey design: the evolutionary study of the cluster-cluster correlation function and of the cluster number density. The adopted XM M observing configuration consists of an equatorial mosaic of 10 ks pointings, separated by  $20^0$  and covering  $8^{\circ} \times 8^{\circ}$ , giving a sensitivity of  $3 \times 10^{-15}$  erg cm $^{-2}$  s $^{-1}$  in the [0.5-2] keV band. This will yield more than 800 clusters of galaxies and a sample of X-ray AGN with a space density of about  $250 \text{ deg}^{-2}$ . We present the expected cosmological implications of the survey in the general context of CDM models and cluster evolution. The XM M -LSS survey is associated to several other major surveys, ranging from the UV to the radio wavebands which will provide the necessary resources for X-ray source identification and further statistical studies. In particular, the associated CFHTLS weak lensing and AMICA Sunyaev-Zel'dovich surveys over the entire XM M -LSS area, will provide for the first time a coherent study of the mass distribution and of cluster physics in the universe on scales of a few hundreds of Mpc. We describe the main characteristics of our wavelet based X-ray pipeline and source identification procedures, including the classification of the cluster candidates by means of a photometric redshift analysis. This permits the selection of suitable targets for spectroscopic follow-up. We present the preliminary results pertaining to the first 15 XM M -LSS pointings: X-ray source properties, optical counterparts, highlights from the first Magellan and VLT/FORS2 spectroscopic runs as well as preliminary results from the NIR search for  $z > 1$  clusters. The results are promising and, so far, in accordance with our predictions as to the survey sensitivity and cluster number density. The feasibility of the program has been demonstrated and further X-ray coverage is awaited in order to proceed with a truly significant statistical analysis.

**Key words.** X-ray, Large Scale Structures, clusters of galaxies, AGN

## 1. Introduction

### 1.1. The role of clusters in cosmology

We have come a long way since the Virgo cluster of galaxies was discovered as an accumulation of "nebulae" (Messier 1781), the first time the term "cluster" was used (Shapley & Ames 1926), and the first inference of large amounts of "dark matter" in the Virgo cluster (Zwicky 1933), to the point where clusters of galaxies are now routinely used as cosmological tools. This progress, is intimately related to the development and success of the standard cosmological model over the past 50 years, following ever-deeper insights into the early evolution of the Universe and the growing power of numerical simulations. From a simple theoretical point of view, clusters of galaxies – the most massive bound structures in the Universe – are objects having a mass of the order of  $10^{14-16} \text{ M}_\odot$  growing by accretion at a rate governed by the initial density fluctuation spectrum, the cosmological parameters, the nature and amount of dark matter as well as the nature of the dark energy. Their 3-dimensional space distribution and number density as functions of cosmic time constrain cosmological parameters in a unique way. Non-gravitational effects accompanying cluster formation render the picture more complicated, but compared to galaxies, clusters still offer considerable advantages for large scale structure (LSS) studies: they can provide complete samples of objects over a very large volume of space, and they are in crucial respects simpler to understand. The extent (and mass) of clusters can be traced by their X-ray emission while the theory describing their formation (biasing) and evolution from the initial fluctuations can be tested with numerical simulations. Such a level of understanding does not exist for galaxies – which have reached a highly non-linear stage – to and even less for QSO and AGN formation. The resulting cluster LSS counts studies can constrain cosmological parameters, independently of Cosmic Microwave Background (CMB) and supernova (SN) studies since they do not rely on the same physical processes. In addition, they can also be used to test fundamental assumptions of the standard paradigm, such as the gravitational instability scenario. A quantitative overview of the cosmological implications of cluster surveys can be found for instance in Haiman et al 2001.

Conversely, given a cosmological model, a large and deep statistical sample of clusters would provide long-awaited information linking cluster physics, non-linear phenomena involved in cluster evolution, and scaling relations. Further, cluster number counts as a function of both the redshift and X-ray luminosity (or any observable), provide strong consistency tests on assumptions made in modelling the mass-luminosity (or mass) relation and cosmological models involving dark energy (Hu 2003). This is very timely, since following

the WMAP<sup>1</sup> results, independent cosmological constraints from both the early and the local universe, must be integrated into a consistent framework.

### 1.2. The quest for clusters

Initiated by Abell (1958) over the whole sky in the optical, the systematic search for clusters underwent a boost of activity in the X-ray waveband during the Einstein (1978–1981) era. The first X-ray rockets and satellites had revealed the existence of X-ray emission associated with clusters. The Uhuru (1970) data, in particular, showed that this emission is thermal and originates in a hot diffuse gas trapped in the gravitational potential of the cluster. The Extended Einstein Medium Sensitivity Survey (EMSS<sup>2</sup>) provided some 730 serendipitous X-ray sources extracted from pointed observations down to a sensitivity of  $1.5 \times 10^{-13} \text{ erg cm}^{-2} \text{ s}^{-1}$  in the [0.3–3.5] keV band. A sub-sample of 67 sources identified as clusters of galaxies in the  $0.1 < z < 0.6$  range, (Gioia et al 1990) suggested, for the first time, a mild evolution in the cluster number density. Next, the ROSAT All-Sky-Survey<sup>3</sup> (RASS, 1990–1991) provided the first sample of X-ray clusters over the entire sky (with an average PSF of  $2^0 \text{FWHM}$ ) and thus, a fundamental resource for LSS studies. Cosmological implications have been investigated in detail from the southern REFLEX ( $3 \times 10^{-12} \text{ erg cm}^{-2} \text{ s}^{-1}$  in the [0.2–2.4] keV band) and North Ecliptic Pole samples (down to  $3 \times 10^{-14}$ ) by Boehringer et al 2001 and Henry et al 2001 respectively.

In parallel, following on the EMSS achievement, serendipitous searches for distant clusters in deep pointed ROSAT observations led to the discovery of clusters out to  $z = 1.2$  with a modest evolution of the bulk of the high luminosity X-ray cluster population; a summary of the main X-ray cluster surveys is presented on Fig. 1.

Both approaches are consistent with hierarchical models of structure formation in a flat low density universe with  $\Omega_m = 0.3$  and the matter density and the amplitude of mass fluctuations on  $8 \text{ h}^{-1} \text{ Mpc}$  scale,  $\sigma_8 = 0.7 \pm 0.8$  (see Rosati et al 2002, for a review). In parallel, the quest for clusters in the optical made its own way, from automated searches on digitised sky survey plates to deep multi-colour CCD imaging. Indeed, beyond  $z = 0.8$ , detecting clusters only from galaxy overdensity in a single band is severely hampered by the faint background population, so that the use of *ne-tuned* photometric redshift information becomes mandatory (see e.g. Sec. 4.2). However, given the limitations on the accuracy of such methods and various underlying hypotheses about galaxy evolution, this usually yields large numbers of high- $z$  candidates, many of them simply being portions of cosmological filaments seen in projection. One will thus always expect – beside extensive optical spectroscopic campaigns – an ulti-

Send off print requests to: M. Pierre, m.pierre@cea.fr

<sup>2</sup> paper based on observations obtained with the XMM-CH, ESO, VLA, CTIO and Las Campanas observatories

<sup>1</sup> [http://lambda.gsfc.nasa.gov/product/map/map\\_bibliography.html](http://lambda.gsfc.nasa.gov/product/map/map_bibliography.html)

<sup>2</sup> <http://xmlgsfc.nasa.gov/archive/catalogs/9/9015/>

<sup>3</sup> <http://heasarc.gsfc.nasa.gov/docs/rodat/survey/>

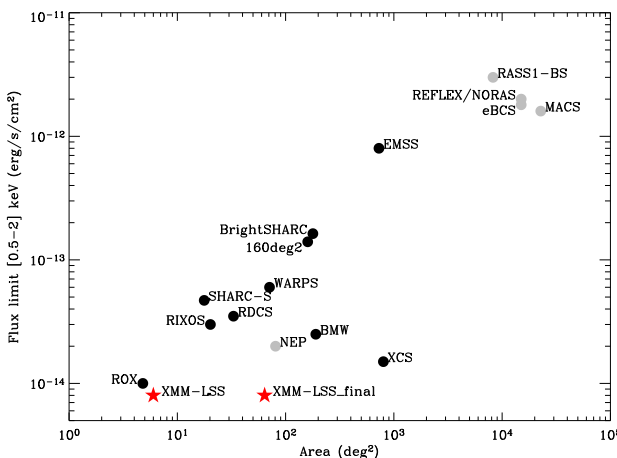


Fig. 1. Overview of existing X-ray cluster surveys as a function of coverage and limiting flux. The light filled circles indicate surveys covering contiguous area, while the dark circles represent serendipitous surveys; the stars show the position of the survey presented in this paper, the XMM-LSS survey (current stage and the foreseen final coverage). References: MACS (Ebeling et al 2001), RASS1-BS (de Grandi et al 1999), eBCS (Ebeling et al 2000), REFLEX/NORAS (Bohringer et al 2000, 2001), EMSS (Gioia et al 1990), XCS (Romer et al 2001), BMW (Panzera et al 2003), Bright SHARC (Romer et al 2000), 160deg² (Vikhlinin et al 1998), NEP (Henry et al 2001), WARPS (Perlmutter et al 2002), RDGS (Rosati et al 1998), RIXOS (Castander et al 1995), SHARC-S (Collins et al 1997), ROX (Donahue et al 2001).

mate contamination from the X-ray band, in order to assess the presence of deep potential wells.

### 1.3. The power of XMM

At the time the XMM project was initiated<sup>4</sup>, the case for surveys was not as compelling as it is today. Ten years after the completion of the RASS, and following considerable steps forward in our knowledge of cluster physics (e.g. Peterson et al 2002), XMM is in a position to open a new era for X-ray surveys. Its high sensitivity, considerably better PSF than the RASS (6<sup>00</sup> on axis) and large field of view (30<sup>0</sup>), make it a powerful tool for the study of extragalactic LSS. In this respect, two key points may be emphasized. Firstly, a high galactic latitude field observed with XMM at medium sensitivity ( $0.5 \times 10^{-14}$  erg cm<sup>-2</sup> s<sup>-1</sup>) is "clean" as it contains only two types of objects, namely QSOs (pointlike sources) and clusters (extended sources) well above the confusion limit. Secondly, if clusters more luminous than  $L_{[2-10]} \gtrsim 3 \times 10^{44} h_{70}^{-2}$  erg/s are present at high redshift, they can be detected as extended sources out to  $z = 2$ , in XMM exposures of only

<sup>4</sup> First discussions proposing some 27 telescopes in 1982; acceptance in 1988

10 ks. XMM is a powerful wide angle X-ray imager, with a sensitivity to extended sources which will remain unrivaled in the coming decade. In parallel, progress in optical wide field imaging provides the necessary resources for the identification of faint X-ray sources. Consequently, we are now in a position to probe the evolution of the cosmic network traced by clusters and QSOs over large volumes of the Universe to high redshift.

### 1.4. The goals of the XMM-LSS

Each new generation of instruments brings – in some respect – at least one order of magnitude improvement compared to its predecessor. While REFLEX was the first X-ray survey to systematically address LSS with clusters in the nearby universe (450 clusters with  $z = 0.2$ ), there is now a clear need to investigate the evolution of the cosmic network out to  $z = 1$ . In this context, we have designed a survey to yield some 800 clusters in two redshift bins with  $0 < z < 1$ : the XMM Large Scale Structure Survey (XMM-LSS). This simple goal has set the sensitivity and the coverage of the XMM-LSS and, as shown in Sec. 2.1, implies an X-ray sensitivity about 3 orders of magnitude deeper than REFLEX. Consequently, this survey will determine how the cluster number density evolves – a hotly debated topic. It will also trace the LSS as defined by X-ray QSOs out to redshifts of  $\sim 4$ . The cosmological implications of the XMM-LSS are summarized in Sec. 2. In addition, the proposed X-ray survey is associated with several other major new generation surveys (optical, IR, Radio, UV). This will provide a new data set that can be used to study the evolution of clusters, cluster galaxies, and of star and AGN formation as a function of environment, in the context of structure formation. An overview of these capabilities is presented in Sec. 3. In the following sections we present a summary of results derived from the XMM AO-1 data set, demonstrating the feasibility of the project. Specifically, in Sec. 4, we describe our current X-ray source identification procedure, which led to the first spectroscopic and NIR follow-up campaigns in Autumn 2002 (Sec. 5 & 6). Future activities and immediate improvements are presented in Sec. 7.

### 1.5. The XMM-LSS consortium

The wide scope of the project has motivated the assembly of a large consortium to facilitate both the data reduction/management and the scientific analysis of the survey. The XMM-LSS Consortium comprises some fifteen European and Chilean institutes. The project is presented in detail on the following website: [http://vela.astro.ulg.ac.be/themes/spatial/xmm/LSS/index\\_en.html](http://vela.astro.ulg.ac.be/themes/spatial/xmm/LSS/index_en.html)

## 2. Survey design and cosmological implications

### 2.1. Defining the survey

Given our driving goal of extending the REFLEX achievements to high redshift (Sec. 1.4), the following objectives were decisive in designing the survey.

Measure the cluster correlation function in two redshift bins spanning  $0 < z < 1$ , with a good level of accuracy. This implies a minimum of about 400 clusters for each bin.

Probe a comoving length which is significantly larger than  $100 h^{-1} Mpc$  at  $z = 1$ , the characteristic scale in the galaxy power spectrum of the local universe (e.g. Landy et al 1996). This constraint corresponds to an opening survey angle of  $10^\circ$  at  $z = 1$  (i.e.  $400 h^{-1} Mpc$ ).

Find the best compromise between the two above constraints in order to minimize the necessary XM-M observing time. Quantitatively, we used the Press-Schechter formalism (Press & Schechter 1974) and the mass-temperature relation from simulations to predict the counts of clusters and their X-ray properties in several CDM models (Refregier et al 2002). We computed the detection efficiency of clusters, using realistic simulations of XM-M images, and studied how this differs from a conventional flux limit. In order to fulfill the first 3 conditions above, and assuming the current favoured CDM cosmological model, the optimal survey design was found to be an  $8^\circ \times 8^\circ$  area, paved with 10 ks XM-M pointing separated by  $20^\circ$  apart (i.e. 9 pointings per  $deg^2$ ). The expected ultimate sensitivity is  $3 \times 10^{-15} erg cm^{-2} s^{-1}$  for pointlike sources in the  $[0.5-2]$  keV band. This is about 1000 and 10 times deeper than the REFLEX (Bohringer et al 2001) and NEP (Henry et al 2001) single area surveys respectively and provides much better angular resolution ( $6^\circ$  vs  $2^\circ$ ).

Find an adequate survey location. An equatorial field is optimal, as ground-based follow-up resources from both hemispheres may be used. High galactic latitude and the absence of bright X-ray sources (e.g. nearby clusters) are also required. Moreover, the visibility of the field by XM-M must be  $> 15\%$ . Given this, only one area in the sky turned out to be favorable: a field centred around  $\alpha = 2^h 18^m 00^s$ ,  $\delta = +7^{\circ}00'00''$  (at  $b = +58^\circ$ ) with neutral hydrogen column  $2 \times 10^{20} < N_H cm^{-2} < 5 \times 10^{20}$ . Whereas this region appears to be the best compromise between many astronomical and instrumental constraints, it should be noted that it is not optimal for far infrared observations (above  $25 \mu m$ ) because of cirrus contamination. The X-ray survey is centred on two deeper areas (one and two square degrees) deriving from XM-M guaranteed time programs (GT). Several surveys are located in the same region (Sec. 3) of which an overview map is presented on Fig. 2.

Fig. 2. Large white square indicating the location of the XM-M-LSS survey is overlaid on a map of  $N_H$  ( $1.4 \times 10^{20} < N_H < 3.5 \times 10^{20}$  for the XM-M-LSS field). The survey area surrounds two deep XM-M surveys based on guaranteed time: the XM-M-SSC/Subaru Deep Survey (80 ks exposures in  $1^\circ$ ) and the XM-M Medium Deep Survey (XMDS; 20 ks exposures in  $2^\circ$ ) also corresponding to the VIRMOS-DESCART Deep Survey [deep], the latter being a collaboration between several instrumental teams: XM-MOM (Liege), XM-M-EPIC (IAS-FMI/LANL), XM-M-SSC (Saclay), CFHTLS (Saclay, IAP), VIRMOS (LAM, IAS-FMI/LANL, OAO). The area overlap will greatly assist in quantifying the completeness of the survey. Also indicated, are the positions of the associated DESCART-VIRMOS Deep Survey [wide], the SWIRE SIRTF Legacy Survey and the NOAO deep survey (Sec. 3). Note that the center of the whole XM-M-LSS survey has been shifted by  $2^\circ$  southward from its initial position because of the presence of the variable type M7 star Mira Ceti (02 19 20.8-02 58 39) which can reach  $I=1$ , thus very dangerous for the optical mapping.)

### 2.2. Constraining cosmology - Quantitative assessments

The prospects that the XM-M-LSS cluster catalogue offers for determining cosmological parameters have been

Fig. 3. First view of the deep X-ray sky on large scales. Image obtained combining the first 15 XMM-LSS fields mosaiced in true X-ray colours: red [0.3-1.0] keV, green [1.0-2.5] keV, blue [2.5-10.0] keV. The circles indicate the sources found in the RASS; the brightest one being a star, HD 14938. The displayed region covers 1.6 deg<sup>2</sup>. This is the first time that such an X-ray depth has been achieved over such an area. The improvement with respect to the RASS is striking, with a source density of the order of 300 deg<sup>-2</sup> in the [0.5-2] keV band. The wealth of sources includes supersoft and very hard sources, as well as sources with a wide range of intrinsic extents, giving an indication of the scientific potential of the XMM-LSS survey.

studied in detail by Refregier et al. 2002. We recall here the main issues.

The cluster counts set strong constraints on the value of the  $m_8$  combination. This combination will also provide a consistency check for the CDM model, and a discrimination between this model and the OCDM model.

The addition of the cluster 2-point correlation function provides a constraint on  $\sigma_8$ , the shape of the initial density fluctuation power spectrum.

With the current survey design, the simultaneous expected precision on  $m_8$  and  $\sigma_8$  is about 15%, 10%, 35% respectively. It is important to note that the present uncertainties on  $\sigma_8$  globally result in a factor of 2 uncertainty in our predicted cluster numbers of 15 deg<sup>-2</sup> (i.e. from 600 to 1200 clusters detections expected within  $0 < z < 1$ ). The high sensitivity to  $\sigma_8$  is not surprising, as it is precisely this which makes cluster counts a good measure of this parameter. This uncertainty can be reduced by analysing about 15 deg<sup>2</sup> of the XMM-LSS, the minimum

area required to improve upon the current measurements of  $\sigma_8$  in the presence of shot noise and cosmological variance.

The sensitivity of the XMM-LSS survey allows the entire cluster population ( $> 2$  keV) to be detected out to a redshift of 0.6, and will unveil the nearby group population. Rather few galaxy groups have been well-studied in the nearby universe, whereas they are believed to constitute the majority of the mass, and of the baryon reservoir. They are also the building block of richer clusters. With increasing redshift, the XMM-LSS is less sensitive to low mass systems. Consequently, the low- $z$  and high- $z$  samples to be used for the study of the LSS, will pertain to different cluster mass ranges. But as outlined above, this does not prevent the derivation of strong cosmological constraints. Further, in a more comprehensive approach, the XMM-LSS high- $z$  clustering properties will be compared to the REFLEX ones, which accurately sample the most massive nearby clusters.

### 3. Associated multiwavelength surveys: an overview

While optical information remains the primary data base for X-ray source identification, contribution from other wave bands may be critical, for example in the far infrared domain, where many heavily absorbed X-ray QSO, not visible in the optical, are expected to show up. Beyond the necessary identification step, multiwavelength information provides an overview of the energy emission and absorption processes in astronomical objects, which is vital to our understanding of their physics, formation and evolution. The contiguous design of the XMM-LSS, optimised for large scale studies, provides considerable advantages for complementary observations, compared to serendipitous fields, and the project has developed numerous collaborations at other wavelengths. The main characteristics of associated surveys are summarised in Table 1 and their main science applications are outlined below.

**Optical, NIR and UV imaging:** The imaging of the 8 deg<sup>2</sup> XMM-LSS area is one of the priorities of the Canada-France-Hawaii Legacy Survey<sup>5</sup> (CFHTLS). It will be performed by Megacam, the one degree field imager built by CEA and installed at the new CFHT prime focus. Imaging of the XMM-LSS region will start by mid 2003. The CFHTLS will provide the deep high quality optical multi-colour imaging counterpart of the X-ray sources at a rate of 25 deg<sup>2</sup>/yr in at least three colours. Data pipelines and processing have been developed by the TERAPIX<sup>6</sup> consortium which provides object catalogues and astrometric positions for the entire surveyed region. Currently, the optical data used for the identification work, and presented in this paper, mostly pertain to the CFH12K VIRMOS-DESCART VLT Deep Surveys (VVDS [deep] and [wide], Fig. 2 and Tab. 1, (Le Fèvre et al. 2003)). An optical cluster catalogue is under construction using the CFH12K (and later Megacam) observations using both spatial clustering analysis and multi-colour matched filter techniques, in addition to photometric redshift estimates. Moreover, the Megacam data will form the basis of a weak lensing analysis<sup>7</sup>, whose cosmological constraints will be compared to those provided by the X-ray data on the same region. This will be the first, coherent study of LSS on such scales. R and z' imaging taken by us at CTIO are also being analysed, forming the basis of an independent cluster catalogue (Sec. 5.1, Andreon et al. 2003). In addition, deep NIR VLT imaging (J & K) of  $z > 1$  cluster candidates found in the XMM-LSS is performed as a confirmation prior to spectroscopy. Finally, a sub area of 8.5 deg<sup>2</sup> of the XMM-LSS field is a high priority target of the Deep Extragalactic Survey part of the UKIRT Deep Sky Survey (UKIDSS<sup>8</sup>). In the UV domain, the XMM-LSS field will

be one of the targets of the Galex<sup>9</sup> Deep Survey, whose main goal is to map the global history of star formation out to  $z = 2$ .

**Spectroscopy:** The standard spectroscopic follow-up is designed to perform redshift measurements for all identified  $0 < z < 1$  X-ray clusters in MultiObject-Spectroscopy mode, using 4m and 8m class telescopes. Current identification procedures and first results are described in later Sections. We shall subsequently undertake programmes of advanced spectroscopy that will focus on individual objects, and include high resolution spectroscopy, the measurement of cluster velocity dispersions and QSO absorption line surveys, as well as NIR spectroscopy of our  $z > 1$  cluster candidates.

**Radio:** In the radio waveband, the complete survey region is being mapped using the VLA at 74MHz and 325MHz. First results of this low frequency coverage are described by Cohen et al. 2003. Radio observations are not only particularly relevant for tracing merger events triggered by structure formation, but also as a useful indicator of galactic nuclear or star formation activity.

**Sunyaev-Zel'dovich:** Observations (S-Z) are also planned. Clusters in the XMM-LSS field will be targets of the prototype O-CRA (One-Centimetre Radiometer Array) instrument. The full XMM-LSS field will be mapped by the O-CRA (in 2004-2004), and will be an early target of the Array for Micro-wave Background Anisotropy (AMBA) (Liang 2001). This will enable not only the measurement of the Hubble constant, but also a statistical analysis of the physics of the ICM as a function of redshift. In the long term, these observations will also provide invaluable information on the low density structures such as cluster outskirts and groups, and their connections to supercluster haloes. These measurements are complementary to the X-ray and weak lensing surveys, connecting the mass distribution of clusters to the structure of the hot gas they contain. The three data sets together will also provide a direct and independent check of the extragalactic distance scale.

**Infrared:** In the infrared, the SWIRE<sup>10</sup> SIRTF Legacy Programme will cover 9 deg<sup>2</sup> of the XMM-LSS in 7 MIR and FIR wavebands from 4 to 160 m (Lonsdale et al. 2003). The estimated IR source densities per square degree in this area are around 1100/400/130 and 670/150/130 for starbursts/spiral-irregular/AGN in the  $0 < z < 1$  and  $1 < z < 2$  redshift intervals, respectively (Xu et al. 2003). This represents a unique X-ray/IR combination in depth and scales to be probed. The coordinated SWIRE/XMM-LSS observations will clarify an important aspect of environmental studies, namely how star formation in cluster galaxies depends on distance from the cluster centre, on the strength of the gravitational potential, and on the density of the ICM. In this respect the XMM-LSS represents the optimum SWIRE field, where galaxy environment, deep NIR imaging and

<sup>5</sup> <http://cdsweb.u-strasbg.fr:2001/Science/CFHLS/>

<sup>6</sup> <http://terapix.iap.fr>

<sup>7</sup> <http://www.iap.fr/Laboeuvre/Activites/TremesRecherche/Lentilles/LentillesTop.htm>

<sup>8</sup> <http://www.ukidss.org/>

<sup>9</sup> <http://www.srl.caltech.edu/galextech/galex.htm>

<sup>10</sup> <http://www.ipac.caltech.edu/SWIRE>

Observatory/Instrument	(Planned) Coverage	Band	Final Sensitivity
XMM /EPIC	64 deg <sup>2</sup>	[0.2-10] keV	$3 \times 10^{-15}$ erg cm <sup>-2</sup> s <sup>-1</sup> [1]
CFHT /CFH 12K (VVDS Deep) *	2 deg <sup>2</sup> GT	B, V, R, I	26.5, 26.0, 26.0, 25.4 [2]
CFHT /CFH 12K (VVDS Wide) *	3 deg <sup>2</sup> GO	V, R, I	25.4, 25.4, 24.8 [2]
CFHT /MegaCam	72 deg <sup>2</sup>	u*, g*, r*, i*, z*	25.5, 26.8, 26.0, 25.3, 24.3 [3]
CTIO 4m /Mosaic	16 deg <sup>2</sup>	R, z*	25, 23.5 [4]
UKIRT /WFCAM	8.75 deg <sup>2</sup>	J, H, K	22.5, 22.0, 21.0 [5]
VLA /A-array *	110 deg <sup>2</sup>	74 MHz	275 mJy/beam [6a]
VLA /A-array	5.6 deg <sup>2</sup>	325 MHz	4 mJy/beam [6b]
OCRA	all XM M -LSS clusters	30 GHz	100 mJy [7]
AMIBA	70 deg <sup>2</sup>	95 GHz	3.0 mJy [8]
SIRTF /IRAC (SWIRE Legacy)	8.7 deg <sup>2</sup>	3.6, 4.5, 5.8, 8.0 m	7.3, 9.7, 27.5, 32.5 Jy [9a]
SIRTF /MIPS (SWIRE Legacy)	8.9 deg <sup>2</sup>	24, 70, 160 m	0.45, 6.3, 60 mJy [9b]
Galex	20 deg <sup>2</sup>	1305-3000 Å	25.5 [10]

Table 1. XM M -LSS X-ray and associated surveys Notes: \* : complete [1]; for pointlike sources in [0.5-2] keV [2]; AB<sub>M</sub> ag, 5<sup>00</sup> aperture [3]; S/N = 5 in 1:15<sup>00</sup> aperture [4]; 4 sigma in 3<sup>00</sup> aperture [5]; Vega<sub>M</sub> ag [6a]; 30<sup>00</sup> resolution; deeper observations planned [6b]; 6:3<sup>00</sup> resolution [7] 5 , detection limit [8] 6 , detection limit [9a] 5 [9b] 5 [10]; AB<sub>M</sub> ag

optical spectroscopic properties will be the main parameters in modelling the MIR/FIR activity. Here also, the location of IR AGNs within the cosmic web will help establish their nature. The FIR/X/optical/radio association will also provide valuable insights into the physics of heavily obscured objects, as well as the first coherent study of biasing mechanisms as a function of scale and cosmic time, for hot (XM M), dark (weak lensing), luminous galactic (optical/NIR) and obscured (SWIRE) material.

In summary, the XM M -LSS multi- data set will offer the first evolving view of structure formation from supercluster to galaxy scales. Its comprehensive approach constitutes a decisive new step in the synergy between space and ground-based observatory resources and therefore a building block of the forthcoming Virtual Observatory.

#### 4. X-ray source lists

In addition to the XMDS Guaranteed Time survey consisting of 18 pointings (Fig. 2), 33 Guest Observer XM M -LSS pointings have been allocated in the first two XM M AOs. At the time of writing (March 2003) all 20 ks GT and 10 ks AO-1 observations have been performed. The preliminary results presented in this section pertain to the first 15 GO XM M -LSS pointings displayed in Fig. 3. Most of the X-ray observations were performed in good conditions. Effective exposure times range from 5 to 16 ks (after removal of bad time intervals, mainly due to ares). The mean exposure time weighted over the area is about 12 ks and 9 ks for the MOS and pn detectors respectively, which is close to the nominal survey exposure time of 10 ks. These contiguous observations were used out to an off-axis angle of 13.3<sup>0</sup> and cover a total area of 1.6 deg<sup>2</sup>.

##### 4.1. Source detection and statistics

The XM M -LSS pipeline (Dos Santos et al. 2003) is based on a 3 stage filtering/detection/measurement process initiated by Valtchanov et al. 2001. After applying the stan-

dard XM M reduction procedure<sup>11</sup>, photon images are generated in several energy bands. These are subsequently wavelet iterated (in counts, to preserve Poisson statistics) computing the significance threshold ( $10^{-4}$ ) in wavelet space by histogram auto-convolution, followed by an iterative reconstruction of the image (M0R1, see Stark & Pierré 1998). The iterated images are then exposure-corrected and a mask map (discarding bad pixels and regions with too low an exposure) is constructed. These steps are performed for each detector independently, allowing us to obtain count-rate images without assuming a spectrum for the sources. Then, the three exposure-corrected images of the same field (MOS1, MOS2 and pn) are summed for the first detection step. SExtractor (Bertin & Arnouts 1996), with parameters adjusted for X-ray iterated images, is then used to obtain a preliminary list of sources. The detection threshold is set to a low value, in order to avoid missing faint sources. The SExtractor source list is then fed into the XM M SAS EM Ldetect task. For each source, this task performs a maximum likelihood PSF fit on each detector independently, thus yielding a quantitative measurement of the source in all detectors, taking into account the PSF variation with energy and off-axis radius, as well as other detector characteristics. The parameters that are varied for each source are: position, number of counts and extension. Position and extension are forced to be the same in each detector, while the number of counts is adjusted to an individual best-fit value for each EPIC instrument. Derived parameters are: source count rate (total and in each instrument), likelihood of detection (total and in each instrument), likelihood of source extent, and extension in arcsec. Since EM Ldetect simply assumes a Gaussian profile for extended sources, we combine the results of SExtractor and EM Ldetect and end up, for each extended source over the detection threshold with several geometrical parameters, including extension, major and minor

<sup>11</sup> [http://xm.m.vilspa.esa.es/external/xmm\\_sw\\_cal/sasframe.shtml](http://xm.m.vilspa.esa.es/external/xmm_sw_cal/sasframe.shtml)

Fig. 4. This image ( $10^0 \times 10^0$ ) provides an overview of the source types encountered in the survey and of the identification procedure. Overlaid on a 1h exposure CFH12K I-band image (processed by Terapix) are blue XM-M flux contours in [0.5–2] keV, obtained by the M-RL multi-scale wavelet filtering algorithm; the procedure allows the automatic recognition of pointlike sources (green squares); the significance of the lowest wavelet contour is  $10^{-4}$  (equivalent to 3.7 for Gaussian noise, cf Starck & Pierre 1998). The image is centred on a bright extended X-ray source, corresponding to an obvious nearby cluster (a NEAR candidate) for which we measured a redshift of 0.33. Another – much more distant – cluster is apparent in the upper left corner (a MID candidate); this object was found to have a redshift of 0.84. Top middle, another extended source without a clear optical counterpart, typically a DISTANT candidate. The density of pointlike sources is high, some of them having an obvious optical counterpart, others, none. The red squares and green circles indicate VLA NVSS and 325 MHz radio sources respectively. In the lower right corner, there is a conspicuous double lobe radio galaxy, which is also an X-ray source.

axis length and principal angle. At this stage of processing, we adopt a conservative approach, retaining all sources detected by EM Ldetect with a maximum likelihood<sup>12</sup> of 8;

source counts being subsequently normalized by the exposure map. We finally select only sources having at least 20 counts (for the 3 detectors, in the [0.5–2] keV band). With the analysis performed on the first 15 pointings, we detect

<sup>12</sup> corrected value: [http://xm-m.vilspa.esa.es/external/xm\\_m\\_new/s/new\\_s.list/xm\\_m\\_new\\_s.029.shtml](http://xm-m.vilspa.esa.es/external/xm_m_new/s/new_s.list/xm_m_new_s.029.shtml)

som e 250 sources per square degree down to a flux limit of  $5 \cdot 10^{-15}$  erg cm $^{-2}$  s $^{-1}$  in the [0.5-2] keV band (assuming a power-law spectrum with a photon index of  $\gamma = 1.7$ ). The current logN -logS curve is shown on Fig. 5.

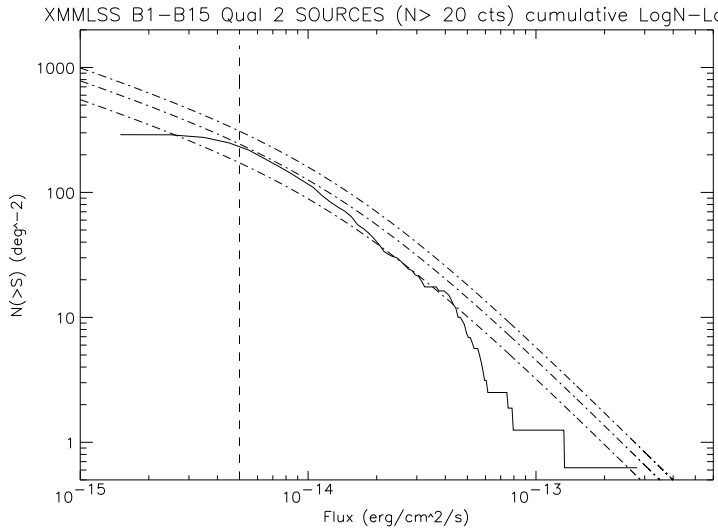


Fig. 5. Cumulative logN -logS distribution, in the [0.5-2] keV band, for the sources pertaining to the first 15 XM M -LSS pointings. The central dot-dashed line is the analytical fit of the deep logN -logS distribution, by Moretti et al 2003, bracketed by the 68% confidence level allowed by the uncertainty on the amplitude of the curve. The apparent lack of bright sources is explained by the small size of the current studied area and the fact that the region has been particularly selected for its low density of bright X-ray sources. Currently the completeness limit is reached around  $5 \cdot 10^{-15}$  erg cm $^{-2}$  s $^{-1}$ . Further refinements of the detection procedure, combined with extensive simulations, should allow us to lower this limit by a factor of two.

#### 4.2. Extended sources and visual check

As clusters of galaxies constitute the core of the project, special care is devoted to the detection and assessment of faint extended sources. The M R1/SExtractor/EM Ldetect hybrid method described above provides a series of parameters used to establish a preliminary list of extended sources. Currently, the procedure is performed on the [0.5-2] keV catalogue which offers optimal sensitivity considering the observed cluster emission spectra over the  $0 < z < 1$  range, the various components of the background (galactic, particle, solar ares), and galactic absorption. We have developed an automated interface to produce X-ray/optical overlays for every extended source candidate (Fig. 4). At the end of the pipeline procedure, each overlay is inspected by eye in order to catch possible instrumental artifacts which could have escaped the pipeline rejection algorithm. Finally, a list of plausible ex-

tended sources is issued with an indication of whether they correspond to an obvious overdensity of galaxies. We currently find an extended source density of about 15-20 deg $^{-2}$ , with conspicuous optical cluster (or group) counterparts on the CFH 12K Images. At this stage, given the small area explored, it is not possible to make statements about these results. The fact that we tend to find somewhat more extended objects than formally predicted, would suggest that either we sample the cluster population below the 2 keV limit that was set in our theoretical predictions, using a given set of M-T-L(z) relations, (a small reduction in the limit to 1.8 keV, could account for this difference); or that we are more sensitive than assumed. An example of the good sensitivity we reach for extended sources is displayed in Fig. 6. This shows that we can tag extended sources down to a flux limit of  $4 \cdot 10^{-15}$  erg cm $^{-2}$  s $^{-1}$  in the [0.5-2] keV band. The study of the logN -logS distribution of extended sources and of their selection function will be the subject of a forthcoming paper.

Fig. 6. The figure shows an XM M source detected as extended with only 50 net counts in the combined image of the 3 detectors. The overlay on the optical image confirms the presence of a distant cluster ( $z = 0.8 - 0.9$ ), and even reveals X-ray structure associated with 2 distinct groups of galaxies. The collected photons correspond to an emitted flux of  $4 \cdot 10^{-15}$  or  $1.2 \cdot 10^{-14}$  erg cm $^{-2}$  s $^{-1}$ , for a source falling on-axis or at an off-axis distance of 11° respectively, assuming a typical thermal cluster spectrum.

#### 5. Source classification

##### 5.1. Clusters

The depths of both the XM M -LSS and of the CFHTLS and CTIO data, have been tuned to sample most of the

cluster population out to a redshift of 1 (Sec. 2.1 and Tab. 1). Beyond this, massive clusters can still be detected in the X-ray band (Valtchanov et al 2001). A cluster located at  $z = 2$  and having a temperature of 7 keV will show up with an apparent temperature of about 2.5 keV, which falls in the most sensitive part of the XM M response. Hence, for such a cluster, the X-ray K-correction is only 0.7 (Jones et al 1998).

In contrast,  $z > 1$  clusters do not appear as significant overdensities of galaxies in the optical band. Increasing the depth of the optical survey would not significantly improve the situation, as most of the galaxy light is shifted into the infrared band. We have therefore adopted the following approach and definitions:

1) A  $z < 1$  cluster candidate is defined as an extended X-ray source corresponding to a significant visual excess of galaxies in the optical wavebands. The multi-colour BVR I $z'$  information is used to enhance the visual contrast of the cluster galaxy density with respect to the background population and to construct optical cluster catalogues following different methods: the Red Cluster Sequence (Gladders & Yee 2000, Andreon et al 2003), clustering analysis in redshift slices (Adami et al 1998), and matched filter (Lobo et al 2000). These catalogues are currently used as ancillary information and cross-correlated with the X-ray extended source catalogue. Further, the optical data allow us to assign photometric redshifts to the X-ray cluster candidates in an independent way. First, we apply the public code Hyperz (Bolzonella et al 2000) to the entire BVR I galaxy catalogue. For each galaxy, we derive the photometric redshift, corresponding to the minimum  $\chi^2$  computed comparing the observed photometric try to the fluxes expected from a set of reference templates (GISSEL 98, Bruzual & Charlot 1993). Second, we search for the cluster signature by placing a number of apertures in the field of the X-ray detection in order to determine the maximum overdensity in photometric redshift space relative to the "field" distribution (Bolzonella et al 2003) and Fig. 7). This approach does not assume that the distribution of cluster galaxy members apparent in the optical data is centred on the X-ray detection and it makes no prior assumption of the apparent optical extent of the candidate cluster. The redshift bin in  $N(z_{\text{phot}})$  has been set similar to the precision expected from photometric redshifts, given the set of filters and their depths (typically  $z = 0.2$ ). Finally, from the region with the largest overdensity detected, we selected the candidate cluster members in different classes of density, considering their  $z_{\text{phot}}$ , their error bars and probability functions. An impressive example of the power of the method is displayed on Fig. 7 and 8. This procedure enables the pre-selection of the cluster candidates into NEAR and MID distance classes, corresponding to the  $0 < z < 0.5$  and  $0.5 < z < 1$  ranges respectively, and provides a useful tool for ascribing targets to the various telescopes available for the spectroscopic follow-up.

2) A small fraction of the extended sources (1 per pointing) do not present any significant optical counter-

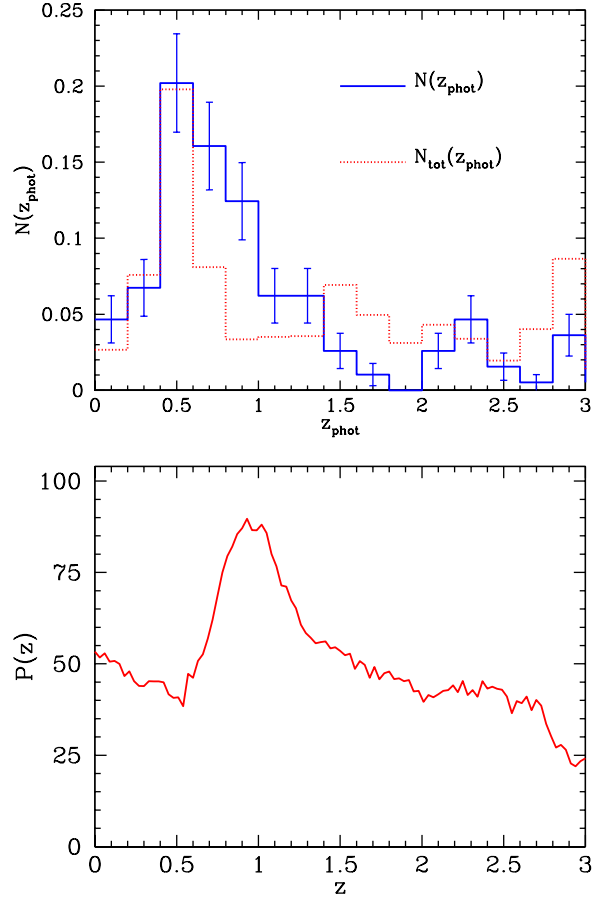


Fig. 7. Photometric redshift determination around the position of an X-ray cluster candidate (see text). Top: the photometric redshift distribution of the region where the overdensity has been detected (solid line), compared to the reference redshift distribution, obtained from the total catalogue (dotted line). The redshift distributions have been normalized to the respective number of objects. To select the significant overdensities, we plot the Poissonian error bars of the small region  $N(z_{\text{phot}})$ . Bottom: combined photometric redshift probability as a function of redshift of galaxies selected within an aperture of radius  $1^0$  whose position within the field maximizes the probability of the redshift "peak". Individual galaxy probabilities are determined from the chi-squared statistic returned from the photometric redshift template fitting procedure (Bolzonella et al 2003). VLT / FORS2 observations showed that this X-ray source indeed corresponds to a structure at  $z = 0.9 \pm 1$ . See Fig. 8

part, occasionally, one or two galaxies visible in the I or  $z'$  band, sometimes nothing at all. These are typically interesting  $z > 1$  cluster candidates and are classified into the third category, DISTANT, to be imaged in the NIR bands. If confirmed, they will be the subject of dedicated spectroscopic follow-up programmes.

pre-selected as described above, comprehensive information (X-ray, optical, photometric redshift) being gathered into an HTM L database, allowing a rapid overview of the cluster properties. From this, we selected a number of clusters spanning different optical morphology and flux ranges, in order to optimise the allocated spectroscopic time, and to give a representative overview of the XM M -LSS cluster population. For the first spectroscopic campaign, it was decided to conservatively obtain two masks per cluster in order to sample well the cluster galaxies in the central region, and ensure consistent redshift determination. Thanks to the high throughput of the FORS2 instrument in the [0.8-1]  $\mu$ m range, all M/LD galaxy clusters candidates were directed to the VLT sample. The NEAR ones were assigned to the Magellan sample, and also as backup sources for VLT, in case of possible low-quality weather conditions. In order to investigate and quantify the most efficient method for the future, galaxies to be measured were selected using different approaches: simple magnitude cut, colour selection or photometric redshift criteria.

Fig. 8. The most distant X-ray complex identified so far, showing a clear concentration of galaxies in the  $0.9 < z < 1$  range (Green X-ray contours overlaid on a CFH12K VRI composite). Bottom right (triangle) is the most distant X-ray QSO currently measured in the XM M -LSS at a redshift  $z = 3.3$  (see Fig. 11); its isophotes are distorted by the immediate vicinity of an X-ray bright emission line galaxy located at  $z = 0.054$ .

## 5.2. AGNs and QSO

Active galactic nuclei constitute by far, the dominant population of X-ray sources at the XM M -LSS sensitivity. Given the XM M PSF, and consequently, the positional accuracy, there is some ambiguity in the identification of pointlike sources, as can be appreciated in Fig. 4 (note the sources having two or three possible optical counterparts, or for which the optical ID is below the limit of the optical survey). This is a well known draw-back, thoroughly studied in deep surveys; but here, the situation is simpler since the XM M -LSS flux limit is well above the confusion limit.

## 6. First spectroscopic campaigns

### 6.1. Strategy

The first spectroscopic observations dedicated to the identification and redshift measurement of the XM M -LSS galaxy clusters took place during the fall of 2002. Three nights were allocated at ESO on the VLT/FORS2 instrument and 2 nights at Las Campanas with the Magellan/LDSS2 instrument. We summarise here the most important outcomes. Galaxy cluster candidates were

No dedicated spectroscopic runs were planned in 2002 for the QSO and AGN population. However, many point-like X-ray sources surrounding the selected clusters and present in the corresponding instrumental field of view were included in the spectroscopic masks. For each  $7^0 \times 7^0$  field centred on a galaxy cluster candidate, we first cross-correlated the X-ray point-like source catalogues with the optical ones obtained from the CFH12K data. We then searched for optical counterparts within a radius of  $5''$  from each X-ray point-like source and produced catalogues of associations. Using the latter, we overlaid on the optical images the positions of the X-ray sources and their associated optical counterparts, if any. Then, we visually checked on the optical images each X-ray position (no more than ten per field) associated with 0, 1 or more optical counterparts. Depending on the "quality" of the X/optical associations, we sorted the AGN/QSO candidates into different categories characterising the priority for spectroscopic observations of the optical counterparts. There were three main classes: (1) unambiguous cases where a unique and relatively bright optical source lies within a radius of  $5''$ ; (2) ambiguous or doubtful cases when there were several possible optical counterparts and/or when the optical counterpart(s) was (were) rather faint; (3) rejected cases when there was no, or a much too faint, optical counterpart. The fraction represented by each class was 35, 25 and 40% respectively. A catalogue containing the first two classes of AGN/QSO candidates was considered for spectroscopic observations of each field. Given the constraints imposed by the cluster spectroscopy (especially, optimal sampling of the cluster cores) and the zones of avoidance within the FORS2 field of view, an average of 2-3 pointlike sources were measured per cluster field. This corresponds to about 30-45 sources per  $\text{deg}^2$ .

## 6.2.0 verview of the results

Weather and working conditions at the VLT were optimal. In three nights, 12 cluster fields (5 M ID, 7 NEAR ( $z > 0.35$ )) were observed, containing on average about 30 slits per mask, yielding some 700 spectra. In addition 2 new nearby compact groups were also observed (with 7 and 8 galaxies per group), prepared as a backup programme. The overall strategy proved successful. An example of spectrum is shown in Fig. 9. Encouragingly, an estimate of the velocity dispersion of a newly discovered 0.84 redshift cluster can be achieved in 2 hours, supporting the follow-up of large numbers of distant clusters with relatively little observing time. Seven NEAR clusters were observed at Magellan, where one night out of the allocated two suffered from poor meteorological conditions. With an average number of slits of 15 per mask, some 200 spectra were obtained.

Current results on the redshift distribution are shown on Fig. 10. Given the selection procedure adopted for this first identification campaign, this cannot be ascribed any cosmological interpretation yet. The photometric cluster distance estimates proved useful and reliable indicators for the cluster classification (cf Fig. 7, 8). A comprehensive X-ray/optical study of the current NEAR and M ID samples is presented by Willis et al 2003 and Valtchanov et al 2003 respectively. The optical properties of the cluster galaxies (luminosity function and colour distribution) are discussed by Andreon et al 2003.

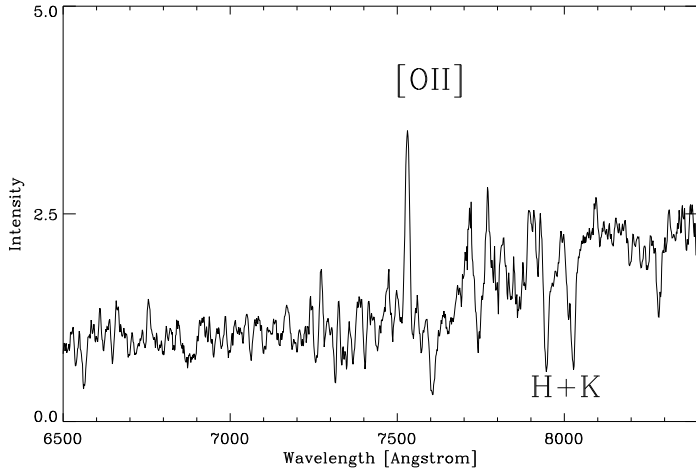


Fig. 9. One of the most distant cluster galaxy measured, at a redshift of  $z = 1.02$  (see Fig. 8). This good quality spectrum was obtained in 1.5h with the R600R+19 grism on the VLT/FORS2 instrument. The object has magnitudes of  $V = 24.19$ ,  $R = 23.34$ ,  $I = 22.21$  and displays characteristics of an elliptical galaxy having a component of young stars (E+A type).

The optical spectra of the measured X-ray AGNs showed a plethora of properties. The most distant X-ray

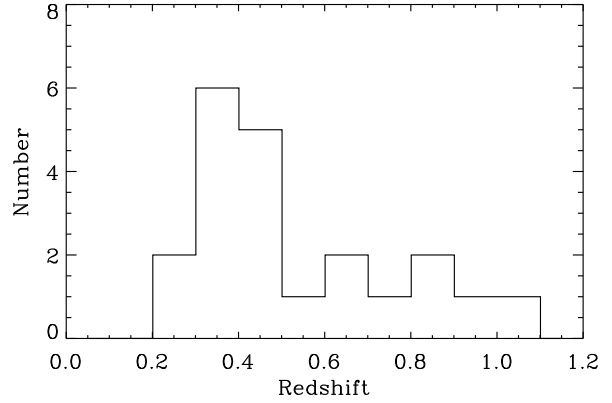


Fig. 10. Redshift distribution of the 19 spectroscopically confirmed clusters during the 2002 Magellan/LDSS and VLT/FORS2 runs.

source measured so far has a redshift of 3.3 (Fig. 11). The AGN sample is currently under analysis (Jean et al 2003).

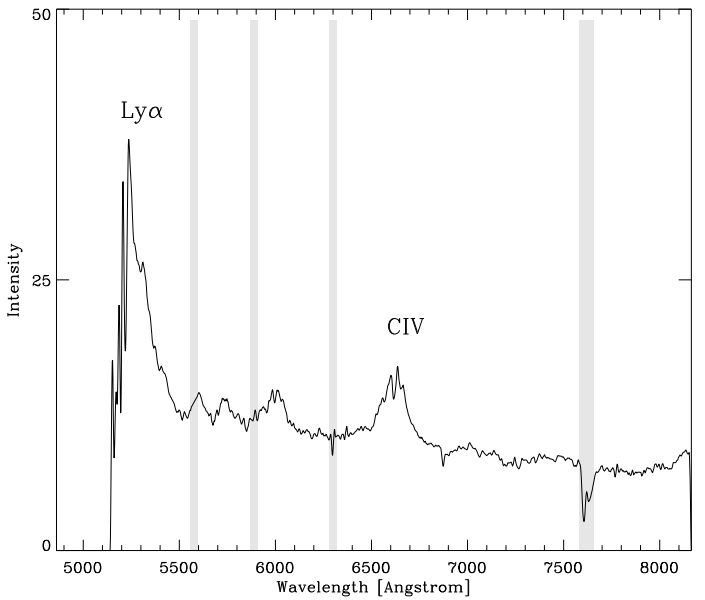


Fig. 11. Most distant X-ray AGN detected so far, at a redshift of  $z = 3.3$  (see Fig. 8); grey bands indicate the position of strong atmospheric lines.

## 7. First NIR imaging campaign

In November 2002, we carried out an initial, exploratory observing run with SOFI on the NTT, in order to search for DISTANT clusters selected from candidates in the first set of available XM M data. The details will be presented elsewhere (Bremmer et al 2003). Here we note that by selecting faint, extended X-ray sources associated with either blank fields in the CFHT data, or with fields showing

a hint of clustering at faint ( $I > 22$ ) magnitude levels in the same data, we were successful at reliably detecting such clusters. Moreover, the X-ray fluxes of these objects are such that if they were placed at higher redshifts they would still be detectable in the XM-M-LSS exposures. Thus the survey will enable us to map the cluster distribution to redshifts well above  $z = 1$ . An example is shown in Fig. 12 and 13.

Fig. 12. Extended X-ray source with a very faint optical counterpart in the I-band. The NIR image of the field is shown in Fig. 13.

## 8. Conclusion and prospects

### 8.1. The newly discovered clusters

Following the completion of the A0-1 period, the main outcome of the XM-M-LSS project can be summarised as follows: XM-M observations of only 10 ks, coupled with a similar time spent on imaging at CFHT or CTIO, can detect a significant fraction of the cluster population out to  $z = 1$  (a flux of  $0.8 \times 10^{14} \text{ erg cm}^{-2} \text{ s}^{-1}$  corresponds to a cluster mass of  $6.7 \times 10^{13} \text{ M}_\odot$  [ $T = 2.7 \text{ keV}$ ] at  $z = 1$ , assuming typical scaling laws). Moreover, adding two hours of FORS2 spectroscopic time, provides a reliable estimate of cluster velocity dispersion at  $z = 0.85$ . This represents a substantial increase in efficiency compared to former high- $z$  cluster searches. The feasibility of the XM-M-LSS programme is now fully demonstrated, and the current data set already provides a valuable sample for cosmological studies. For the first time, we are detecting the number

Fig. 13. J-K colour image of the DISTANT cluster candidate catalogued in Fig. 12. This presents a significant overdensity of red objects. The brightest cluster member has  $K_s = 17.5 \pm 0.3$ , and the other objects within  $20''$  are generally fainter than  $K_s = 18.5$ . These properties are consistent with a cluster at  $z = 1$  or above.

of low luminosity (mass) objects out to  $z = 0.5$ ; this will allow a dense mapping of the matter distribution. So far (within  $4 \text{ deg}^2$ , including the GT area), no massive object has been detected and, following a detailed inspection of the optical images, no giant arcs have been found in the identified clusters. These results are consistent with the Press-Schechter formalism (folded with the current favoured cosmological model) predicting 2.8 and 0.0001 cluster per  $\text{deg}^2$  between  $0 < z < 1$  for clusters more massive than  $10^{14} \text{ M}_\odot$  and  $10^{15} \text{ M}_\odot$  respectively, if we assume that only massive clusters are potential strong lenses. Of course, an additional necessary condition is the steepness of the mass profile.

In immediate foreseen improvements are the following: in the next version of the X-ray pipeline, the source flux detection limit will be significantly lowered. This requires further work on the background estimation. In parallel, extensive simulations are being performed to improve the characterisation (extent and flux) of the faintest sources as well as to determine the survey selection function. This is complicated by the necessity of taking proper account of the Poisson nature of the data and the fact that the signal to be analysed comes from 3 different detectors.

### 8.2. Cluster identification remnants

In a second step, we shall systematically investigate overlaps and differences between the optical cluster catalogues and the X-ray extended source catalogue. There are two main reasons why variations should be observed: (i) faint groups or distant clusters may not be unambiguously de-

tected as extended sources because of their low flux or, alternatively, because they host a cooling flow, which makes them appear unresolved. Currently, we are confident that any regular object having a typical core radius of the order of  $125h_{100}^{-1}$  kpc and producing a net number of counts of 70 is detected by the pipeline as an extended source (Valtchanov et al 2001); (ii) there are intrinsic differences between the X-ray and optical catalogues since the methods used to construct them rely on specific assumptions as to galaxy colour and evolution, or on the properties of the IGM at high redshift. Understanding the discrepancies will not only increase the efficiency of our cluster finding procedure, but also shed light on the much debated topic of cluster formation and evolution. This will also contribute to the improvement of our photometric redshift determination procedure. Finally, output from the weak lensing analysis will reveal large mass concentrations, optimally within the  $0.1 < z < 0.5$  range. Again, the comparison between the X-ray and optical catalogues will be most instructive. Given the current understanding of structure formation, it is difficult to devise a physical process that would prevent gas being trapped or heated within large concentrations of dark matter. However, the surveyed volume is ideally suited to systematically search for 'dark clump'.

### 8.3. Active galactic Nuclei

Due to the primary goal of the spectroscopic observations performed so far (confirmation and redshift determination of X-ray selected galaxy clusters), few AGN/QSO candidates could actually be observed. For this reason, a spectroscopic survey of a unique sample of X-ray selected AGN/QSOs within a large contiguous area of some  $10 \text{ deg}^2$ , typically complete down to  $F_{[2-10]\text{keV}} \sim 10^{-14} \text{ erg cm}^{-2} \text{s}^{-1}$ ,  $F_{[0.5-2]\text{keV}} \sim 5 \cdot 10^{-15} \text{ erg cm}^{-2} \text{s}^{-1}$  and  $I_{AB} = 22.5$  is foreseen. Because of the large surface density of AGN/QSO candidates detected in the XMM-LSS field (typically  $> 200 \text{ deg}^{-2}$  with  $0 < z < 1$ ), compared to previous surveys, it should be more sensitive to contrasts between voids and peaks than previous surveys, such as 2dF. This will enable us to study with high precision the correlation function of these objects over scales in the  $[2-400] \text{ Mpc}$  range, to probe the environmental influence on various type of AGN, and to compare these correlations with those for normal galaxies. The distinct redshift distributions of X-ray selected type I and type II AGN will be very accurately determined, and this will provide interesting constraints on models of black hole formation compared with models of star formation. The proposed studies will provide a comparison of the clustering properties, as a function of redshift, of X-ray, optical (2dF) or radio selected AGN/QSO.

### 8.4. Survey products

A dedicated MySQL database with a Java front end interface is available via a site at IASF Milano<sup>13</sup> with a mirror at ESO Santiago. This will include the X-ray source catalogue, and complete catalogues of surveys performed by the LSS Consortium in other wavebands, together with selected subsets from the surveys performed by other Consortia made available under agreement. It will also give access to a selection of data products. The database, currently accessible and used internally by the Consortium, will be gradually opened to the public. The first public release, based on the A0-1 pointings (X-ray source lists and available identifications) is foreseen for the beginning of 2004.

Acknowledgments. SDS is supported by a post-doctoral position from the Centre National d'Etudes Spatiales. MP and IV are grateful to the ESO/Santiago Office for Science, for a 2 week stay in October 2002, where the analysis of the VLT data presented here was initiated.

### References

Adamic C., Mazzure A., Katgert P., Biviano A., 1998, A & A 336, 63

Andreon S. et al. 2003 in preparation

Amaud, M. & Evrard, A., 1999, MNRAS, 305, 631

Bertin M., Arnouts S., 1996, A & AS, 117, 393

Bohringer, H., Voges, W., Huchra, J.P., McLean, B., Giacconi, R., Rosati, P., Burg, R., Mader, J., Schuecker, P., Simic, D., Komossa, S., Reiprich, T.H., Retzlaff, J., Trumper, J., 2000, ApJS, 129, 435

Bohringer H., Schuecker P., Guzzo L., Collins C.A., Voges W., Schindler S., Neumann D.M., Czerniak R.G., De Grandi S., Chincarini G., Edge A.C., MacGillivray H.T., Shaver P., 2001, A & A 369, 826

Bolzonella, M., Miralles, J.-M. & Pello, R. 2000, A & A 363, 476

Bolzonella et al., 2003, A & A in preparation

Bromer M. et al., 2003 A & A in preparation

Bruzual, G. & Charlot, S. 1993, ApJ 405, 538

Castander, F.J., et al. 1995, Nature, 281, 59

Cohen A. et al. 2003, ApJ submitted

Collins, C.A., Burke, D.J., Romer, A.K., Sharples, R.M., Nichol, R.C., 1997, ApJ, 479, L117

de Grandi, S., Bohringer, H., Guzzo, L., Molendi, S., Chincarini, G., Collins, C., Czerniak, R., Neumann, D., Schindler, S., Schuecker, P., Voges, W., 1999, ApJ, 514, 148

Donahue, M., Mack, J., Scharf, C., Lee, P., Postman, M., Rosati, P., Dickinson, M., Voit, G.M., Stroebe, J.T., 2001, ApJ, 552, L93

Dos Santos et al. 2003, A & A in preparation

Ebeling, H., Voges, W., Bohringer, H., Edge, A.C., Huchra, J.P., Briel, U.G., 1996, MNRAS, 281, 799

Ebeling, H., Edge, A.C., Bohringer, H., Allen, S.W., Crawford, C.S., Fabian, A.C., Voges, W., Huchra, J.P., 1998, MNRAS, 301, 881

Ebeling, H., Edge, A.C., Henry, J.P., 2001, ApJ, 553, 668

<sup>13</sup> <http://cosmos.iiasf.cnr.it/lssadmin/Websit/LSS/>

Ebeling, H., Edge, A. C., Allen, S. W., Crawford, C. S., Fabian, A. C., Huchra, J. P., 2000, MNRAS, 318, 333

Eke, V. R., Cole, S., & Frenk, C. S., 1996, MNRAS, 282, 263

Gioia, I. M.; Henry, J. P.; Macacaro, T.; Morris, S. L.; Stocke, J. T.; Wolter, A., 1990, ApJ Let 356, L35-L38

Gadders, M. D., Yee, H. K., 2000, AJ 120, 2148

Haiman, Z., Mohn, J. J., Holder, G. P., 2001, ApJ, 553, 545

Henry, J. P., Gioia, I. M., M ullis, C. R., Voges, W., Briel, U. G., Boehringer, H., 2001, ApJ Let 553, L109

Hu, W., 2003, astroph/0301416

Jean, C. et al 2003, A & A in preparation

Jones, L. R., Scharf, C., Ebeling, H., Perlman, E., Wegner, G., Malkan, M., Homer, D., 1998, ApJ, 495, 100

Landy, S. D. et al., 1996, ApJ 456, L1

LeFevre, O., Mellier, Y., MacCracken, H. J., Foucaud, S., Gwyn, S., Radovich, M., Dantel-Fort, M., Bertin, E., Cuillandre, J. C., Le Brun, V., Mazure, A., Moreau, C., Pierré, M., Tresse, L., Veillet, C., 2003, A & A, submitted

Liang, H., 2001, astro-ph/0110518

Lonsdale, C. et al 2003, PASP, submitted

Lobo, C., Iovino, A., Lazzati, D., Chincarini, G., 2000, A & A 360, 896

Moretti, A., Campana, S., Lazzati, D., Tagliaferri, G., 2003, astroph/0301555

Panzera, M. R., Campana, S., Covino, S., Lazzati, D., Mignani, R. P., Moretti, A., Tagliaferri, G., 2003, A & A, 399, 351

Perlman, E. S., Homer, D. J., Jones, L. R., Scharf, C., Ebeling, H., Wegner, G., Malkan, M., 2002, ApJS, 140, 265

Peterson, J. R., Ferrigno, C., Kaastra, J. S., Paerels, F. B. S., Kahn, S. M., Jernigan, J. G., Bleeker, J. A. M., Tamura, T., 2002, astro-ph/0202108

Press, W. H., & Schechter, P., 1974, ApJ, 187, 425

Refregier, A., Valtchanov, I., Pierré, M., 2002, A & A 390, 1

Refregier, A., Dos Santos, S., Valtchanov, I., Pierré, M., 2003, in preparation

Romer, A. K., Nichol, R. C., Holden, B. P., Ulmer, M. P., Pildis, R. A., Merelli, A. J., Adam, C., Burke, D. J., Collins, C. A., Metevier, A. J., Kron, R. G., Commons, K., 2000, ApJS, 126, 206

Romer, A. K., Viana, P. T. P., Liddle, A. R., Mann, R. G., 2001, ApJ, 547, 594

Rosati, P., della Ceca, R., Norman, C., Giacconi, R., 1998, ApJ Let 492, 21L

Rosati, P., Borgani, S., Norman, C., 2002, astroph/0209035

Starck, J.-L., Pierré, M., 1998, A & A 128, 397

Sheth, R. K., Tormen, G., 1999, MNRAS 308, 119

Valtchanov, I., Pierré, M., Gastaud, R., 2001, A & A 370, 689

Valtchanov, I. et al 2003, A & A in preparation

Xu, C. K., Lonsdale, C. J., Shupe, D. L., Franceschini, A., Martin, C., Schiminovich, D., 2003, ApJ in press (astro-ph/0212344)

Vikhlinin, A., McDonald, B. R., Forman, W., Jones, C., Quintana, H., Homstrup, A., 1998a, ApJ, 502, 558

W illis, J. et al 2003, A & A in preparation

This figure "fig2.jpg" is available in "jpg" format from:

<http://arxiv.org/ps/astro-ph/0305191v2>

This figure "fig3.jpg" is available in "jpg" format from:

<http://arxiv.org/ps/astro-ph/0305191v2>

This figure "fig4.jpg" is available in "jpg" format from:

<http://arxiv.org/ps/astro-ph/0305191v2>

This figure "fig6.jpg" is available in "jpg" format from:

<http://arxiv.org/ps/astro-ph/0305191v2>

This figure "fig8.jpg" is available in "jpg" format from:

<http://arxiv.org/ps/astro-ph/0305191v2>

This figure "fig12.jpg" is available in "jpg" format from:

<http://arxiv.org/ps/astro-ph/0305191v2>

This figure "fig13.jpg" is available in "jpg" format from:

<http://arxiv.org/ps/astro-ph/0305191v2>